Top Catal (2008) 50:2–18
DOI 10.1007/s11244-008-9096-x

ORIGINAL PAPER

Structures, Mechanisms, and Kinetics of Selective Ammoxidation and Oxidation of Propane over Multi-metal Oxide Catalysts

William A. Goddard III · Kimberly Chenoweth · Sanja Pudar · Adri C. T. van Duin · Mu-Jeng Cheng

Published online: 10 June 2008

Abstract In order to determine the chemical mechanisms for the (amm)oxidation of propane and propene on multi-metal oxide (MMO) catalysts, we have carried out quantum mechanical (QM) calculations for model reactions on small clusters that we have used to train the parameters for the ReaxFF reactive force field, which enables molecular dynamics (MD) simulations for reactions on the complex reconstructed surfaces of MMO. We report here insights from the QM on the reaction mechanisms of selective (amm)oxidation of propene on bismuth molybdate catalysts and the oxidative dehydrogenation of propane on vanadium oxide catalysts. We also report the application of ReaxFF to predict the stable surfaces of the M1 phases of the MoVTeNbO catalysts.

Keywords Multi-metal oxide · MMO · Bismuth molybdate MoVTeNbO · Vanadium oxide · ReaxFF · Reactive force field · Quantum mechanics · Reaction mechanisms · Catalysis

1 Introduction

More than 80% of industrial chemicals produced annually employ catalysts, making it one of the most industrially important chemical processes [1]. Indeed the pressures of modifying industrial processes to reduce environmental impact will increase the need to replace stoichiometric processes in chemical production with catalytic processes. Similarly, improved catalysts are essential to improve energy production processes ranging for combustion to fuel cells.

In particular, multi-metal oxide (MMO) catalysts for selective oxidation and ammoxidation of propene to acrolein and acrylonitrile have been of major commercial importance since the invention of the first ones at SOHIO in ~1955. The products from these catalysts now represent 25% of the chemicals used in the manufacture of industrial and consumer products. A major breakthrough in this area was the invention of new MMO catalysts that successfully ammoxidize propane by Mitsubishi in 1994 and by BP-America (the successor of SOHIO) in 1989 that could selectively convert propane to acrolein and acrylonitrile [2, 3]. Such a catalyst faces significant challenges since the CH bond of propene is 88.8 kcal/mol (weakened by allylic resonance in the product) while the weakest CH bond of propane is 98.6 kcal/mol [4]. A catalyst with a site that can activate a 98 kcal/mol bond might well also activate the CH bonds of the products, increasing the chance of non-selective products such as CO_2. Indeed, despite intensive efforts to develop the MMO propane ammoxidation catalysts, these processes are not yet commercial. Grasselli [5] suggests that current ammoxidation catalysts have a selectivity of 62% whereas at least 70% selectivity would be needed for commercial viability.

This difficulty in achieving commercially acceptable selectivity and activity for these MMO catalysts motivated us to develop theoretical and computational methods suitable for elucidating the mechanism. The idea here is to determine the detailed sequence of atomic level steps that take the propane through various chemisorbed intermediates to the desired products, determining which sites on the catalyst surface are involved in each step and the barriers

W. A. Goddard III (✉) · K. Chenoweth · S. Pudar · A. C. T. van Duin · M.-J. Cheng
Materials and Process Simulation Center (139-74), California Institute of Technology, Pasadena, CA 91125, USA
e-mail: wag@wag.caltech.edu

for the reaction steps. Then, we would also determine the mechanisms (sites and barriers) for production of the undesired side products, such as CO_2. Armed with this information, we would hope that we could provide guidance on modifying the components of the catalysts and the process of catalyst preparation to maximize the selectivity and activity.

This approach has already had some success for understanding the mechanism for the $BiMoO_x$ catalysts for selectively oxidizing and ammoxidizing propene. Thus, in 1985, Allison and Goddard used quantum mechanics (QM) calculations (then quite primitive) to show the role of the spectator oxo and spectator imido effects in promoting the activation of propene and in the subsequent insertion into surface Mo=O and Mo=NH bonds to form the product [6]. This work showed that Mo sites with two oxo or imido bonds are particularly reactive and suggested that two such sites are required for selective oxidation to form acrolein and that four are required to produce acrylonitrile.

By 2000, QM methods had improved dramatically, allowing Jang and Goddard to revisit these mechanisms, as reported at IRSEE-I [7, 8]. They were able to carry out quite accurate calculations on metal oxide clusters (Mo_3O_9 and Bi_4O_6) that mimic sites on the $BiMoO_x$ surface, providing accurate energetics for the various reaction steps. These more accurate energetics allowed some detailed tests of the spectator oxo and imido ideas, which were found to explain the changes in the kinetics of ammoxidation between the low NH_3 and high NH_3 conditions. This work confirmed the mechanistic steps suggested by Allison and Goddard, but provided much more accurate energetics. This led to the mechanism shown in Figs. 1 and 2 that involves:

1. Coordination of propene to the catalyst followed by allylic hydrogen abstraction by Bi^{V} site, resulting in allyl intermediate.
2. The allyl radical adsorbs onto a Mo=O at a $Mo^{VI}(=O)_2$ site to form the C–O bond of the product.
3. A second hydrogen is abstracted by a 2nd $Mo^{VI}(=O)_2$ site to form the acrolein product.

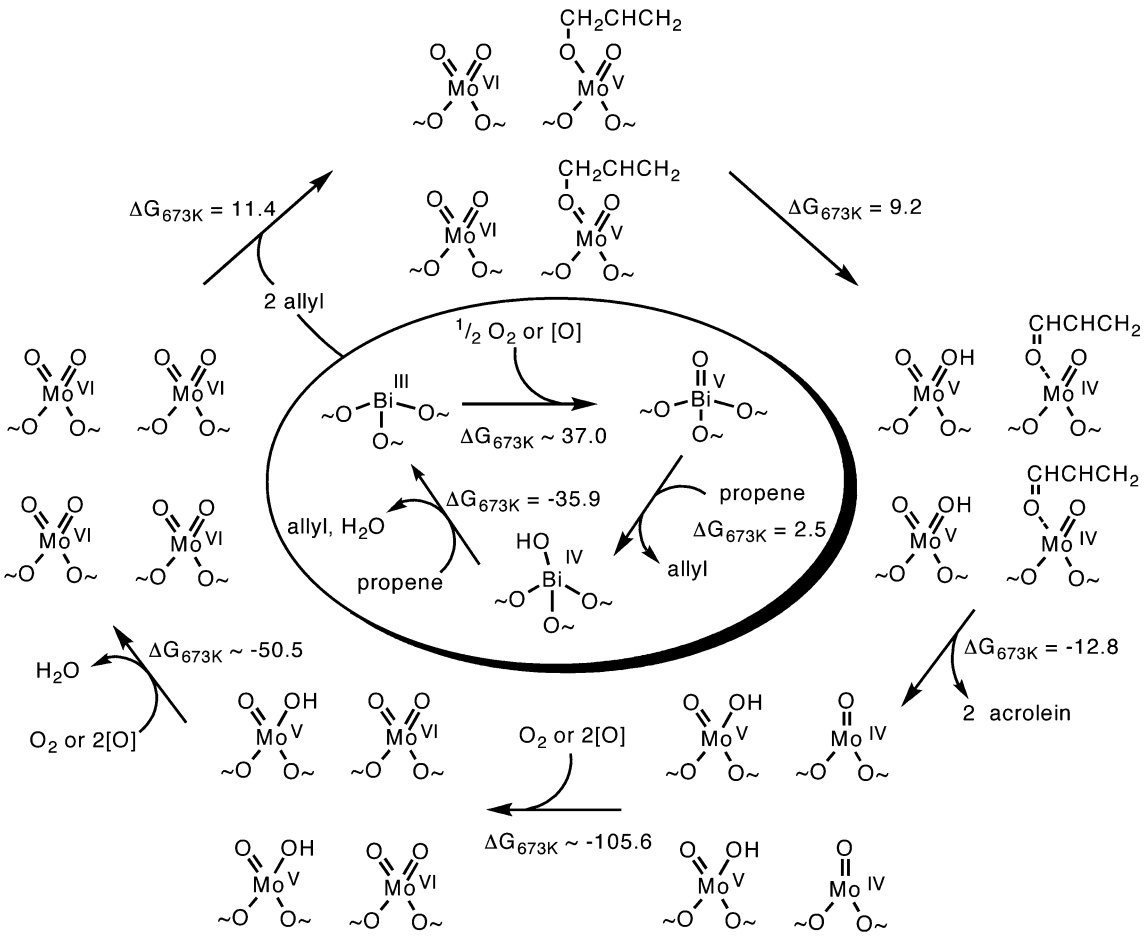

Fig. 1 Mechanism for the selective oxidation of propene to acrolein by $BiMoO_x$. Energies are reported in kcal/mol

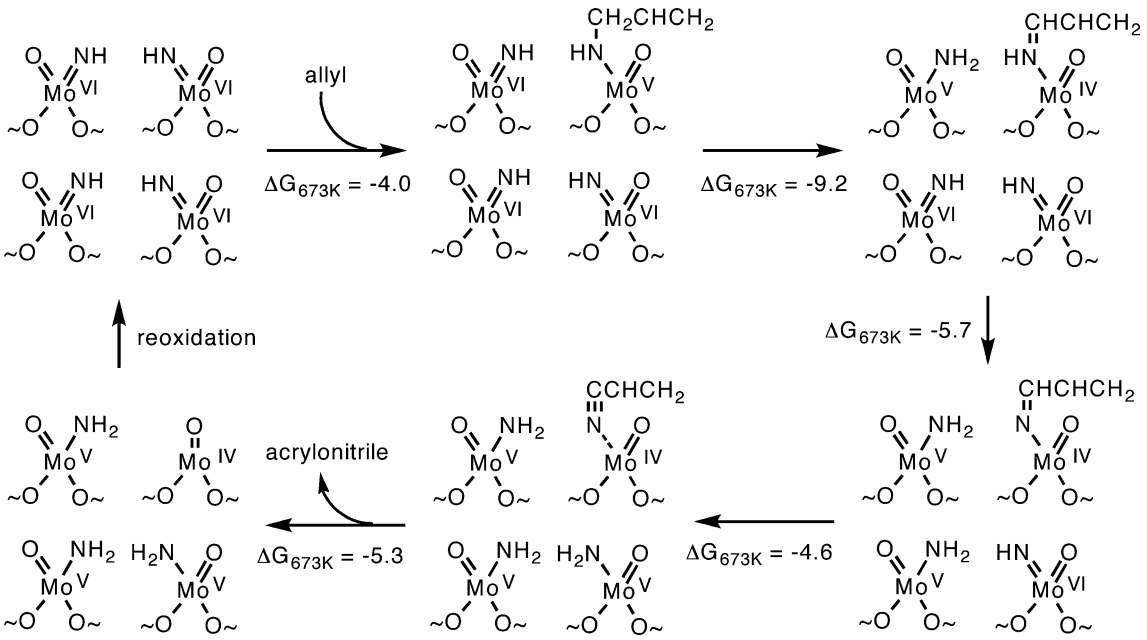

Fig. 2 Mechanism for the ammoxidation of propene to acrylonitrile by $Bi_2Mo_2O_9$. Energies are reported in kcal/mol

4. The ammoxidation mechanism proceeds in essentially the same way as oxidation, except that in step 2, the allyl radical inserts into the Mo=NH bond of a $Mo^{VI}(=NH)_2$ or $Mo^{VI}(=NH)(=O)$ site to form the CN bond of the product.
5. In addition after step 2, a third and fourth hydrogen are abstracted by additional $Mo^{VI}(=NH)_2$ or $Mo^{VI}(=NH)(=O)$ sites to form the acrylonitrile product.

With one exception, the above mechanism is now accepted by the experimental community and was adopted in the review by Grasselli et al. [9] at IRSEE-II in 2002. The only issue is step 1, where the QM calculations found that only Bi^{V} centers can activate the allylic H bond of propene required in the rate-determining step of this process. In contrast, experimentalists have concluded that Bi^{III} centers are involved because bulk $Bi_2Mo_3O_{12}$ is observed to activate a small amount of propene and convert it to hexadiene [10]. This led to a great deal of discussion at IRSEE-I with skepticism from most of the experimentalists. Our speculation is that bulk $Bi_2Mo_3O_{12}$ may have some Bi^{V} sites at the surface (or perhaps some other activated site that can do the activation) under reaction conditions. Certainly $BiMoO_x$, has increased possibilities for Bi^{V} centers.

Although the Jang and Goddard work provided accurate energetics from QM, they were not able to carry out accurate calculations for the various reaction barriers at that time. Moreover it is not clear that such QM calculations based on clusters can mimic the mixed metal oxide sites likely to play a role in ammoxidizing saturated hydrocarbons. The MMO catalysts that successfully ammoxidizes propane have very complex structures with multiple phases, each with 100's of atoms per cell even in the idealized cell obtained from powder x-ray studies [11]. The situation is additionally complicated because the structures derived from powder x-ray studies have partial occupation of the metals at various site, even in the crystal and it is likely that at the surface there will be additional non-stoichiometry and reconstruction. The metals important in these MMOs include Mo, V, Nb, Ta, Te, Bi, with minor amounts of other metals, further increasing the complexity. As a result, experimental techniques have provided insufficient information about the mechanism and progress in improving these catalysts has been very empirical and ineffective.

Grasselli [9, 12] has proposed a mechanism for propane (ammo)oxidation to acrolein and acrylic acid based on empirical catalyst composition/performance information.

1. The active site is composed of a [V–Nb–O$_x$] cluster (analogous to the Bi^{3+} site) that serves as the paraffin H-abstraction site. The oxidation state of the V is most likely V^{5+}.
2. This V site is in proximity to an oxidized [Mo–Te–O$_x$] cluster that is the site for allylic H-abstraction on Te^{4+} centers and for O-insertion on Mo^{6+} centers.
3. The Nb is Nb^{5+}, which is thought to provide structural stability for the V^{5+} phase. Since V^{5+} in the absence of Nb is known to activate paraffins in other catalysts, it seems reasonable that the Nb would serve a promoter role (like Fe in Fe–Sb–O$_x$ catalysts) rather than as the primary H-abstraction site.

4. The mechanism most likely involves propane to propylene conversion, followed by propylene oxidation. Propylene formation involves H-abstraction on V^{5+} sites to form an absorbed 2-propyl radical, which rapidly undergoes a second H-abstraction to form propene.
5. Unlike propylene oxidation, in which activation for the second allylic H-abstraction requires formation of the O-allyl species, the hydrogen abstraction from the 2-propyl radical is much more facile. This is shown as occurring on a Te site in the MoÐTeÐOx cluster, but this could probably occur on almost any oxygenated site in the catalyst.
6. Subsequent oxidation to either acrolein or acrylic acid is very analogous to the BiÐMoÐOx mechanism where Te^{4+} center replaces the Bi. The Te portion of the cluster, in proximity to the Mo allyl-absorption component also provides a site for the second and third allyl abstraction.

We report here a theoretical approach that we have developed to treat systems as complicated as MMO with up to 100,000 atoms per cell. This is the ReaxFF reactive force Þeld, which was developed to provide an accuracy nearly that of QM for reaction pathways and transition states but at a cost nearly as low as for a simple force Þeld. We have used ReaxFF in molecular dynamics (MD) simulations of MMO models of M1 and M2 phases fully equilibrated at correct reaction temperatures to study reactions under realistic conditions. We report here preliminary MD simulations to investigate the atomistic details underlying the mechanisms. We will continue applying this approach to elucidate the mechanism of propene and propane oxidation and ammoxidation catalysts. We expect these simulations to identify new compositions for these catalysts that could exhibit higher rates and selectivities, and we plan to optimize these systems using computational simulations under realistic reaction conditions. We hope that the fundamental understanding of the MMO catalysts resulting from this work will lead to advances in industrial catalysts to obtain improved activity and selectivity at low temperature and pressure conditions. This could lead to cleaner and more efÞcient production of chemicals.

We report here some of the advances in our understanding of selective oxidation and ammoxidation of propene on bismuth molybdate catalysts and the oxidative dehydrogenation of propane on vanadium oxide catalysts. We have used the results from these QM mechanistic studies as well as an extensive QM training set to parameterize a ReaxFF reactive force Þeld which we have employed to study the structure, composition, and reactivity of the stable surfaces of the M1 phase.

2 Methodology

2.1 ReaxFF Reactive Force Field

Over the last Þve years we have been developing the Þrst principles-based ReaxFF reactive force Þelds and have now demonstrated that ReaxFF is capable of reproducing the energy surfaces, structures, and barriers from accurate QM calculations for reactive systems. ReaxFF studies have been reported for a wide range of materials, including hydrocarbons, [13, 14] nitramines, [15] ceramics [16] (Si/SiO_2), metals and metal oxides [17], metal/hydrocarbon interactions [18] and metal hydrides [19] demonstrating that ReaxFF has the versatility required to capture the complexity of the mixed metal catalyst system. ReaxFF includes the following features:

- *Environmentally dependent charge distributions on atoms*. In ReaxFF the Coulomb interaction between two atoms is shielded for small distances so that it can include the electrostatic interactions between bonded atoms (not excluded as common with normal FF). The total magnitude of the charge on each atom is allowed to change depending on the environment. Thus an H next to C is generally positive while a C next to an O is generally positive. The ReaxFF charge parameters, which consist of electronegativity, hardness, and shielding parameter for each element, are optimized to reproduce QM-derived charge distributions. The exact amount of the charge transfer depends on the nature of the atoms and the distances between them, allowing the atom charge distributions to change during reactions to describe the effects of changes in charge distribution on conformational and reactive events [18].
- *Bond order dependent valence terms*. All valence terms (bonds, angles, and torsions) depend on the bond order, providing a smooth description of chemical reactions. The bond orders are determined uniquely from the interatomic distances allowing ReaxFF to recognize and handle the changes in connectivity during reactions. All parameters describing the valence terms are derived directly from QM studies on a large number (1000Õs) of reactions (allowed and forbidden) and are universal.
- *Non-bond or van der Waals interactions*. Most critical in a FF is to properly account for the short range repulsion and steric interactions arising directly from the Pauli principle. To provide the data for this, we obtain the equation of state from QM for bulk phases involving a variety of coordinations. Thus for metals we typically include coordinations of 12 (fcc and hcp), 8 (bcc), 6 (simple cubic), 4 (diamond), and mixed (A15). We use a Morse function (3 parameters) to

describe the short range repulsion and to include long range attraction. These nonbonding interactions are included between *every* atom pair, independent of connectivity. Excessive short-range attractions or repulsions are avoided by including a shielding term in the nonbond potentials.

Furthermore, the following guiding principles were adopted during the development of the ReaxFF reactive potentials:

- *No discontinuities in energy or forces*. Even during reactions, ReaxFF provides a continuous energy and force description, thus allowing proper reactive MD-simulations.
- *Transferable potential*. Each element is described by just one atom type, allowing good transferability of the force field to new systems and avoiding complicated atom type modification during reactions.
- *No predefinition of reactive sites*. With ReaxFF, one does not need to predefine where and when they expect reactions to occur. We typically heat a gas of molecules near a surface and allow the reactions to proceed, allowing unbiased simulations on reactive systems.

2.2 QM-methods

For QM calculations on smaller cluster models, we use the B3LYP flavor of Density Functional Theory (DFT) as implemented in Jaguar 6.5 [20]. The double-ζ quality LACVP** effective core potential and basis set was used to describe V, Mo, Bi, Nb, and Te [21]. For the C, H, N, and H atoms, all electrons were treated explicitly with the Pople 6-31G** basis set [22]. This includes the generalized gradient approximation (Becke non-local gradient correction), exact exchange using the Becke three-parameter exchange functional, [23] and the non-local correlation functional of Lee, Yang, and Parr [24]. We find that the B3LYP flavor of DFT generally provides adequate accuracy at modest cost, reproducing thermodynamics for a wide variety of structures with a mean error of 3 kcal/mol [25]. All stationary points have been identified as local minima (zero imaginary frequencies) or transition states (TS) (one imaginary frequency). Vibrational frequencies have been calculated at all stationary points to obtain zero point energies (ZPE) and free energies at the catalyst operational temperature (600 K). The periodic QM-calculations were performed using the SeqQuest program. This uses the PBE GGA exchange-correlation functional. The Gaussian basis sets were optimized at the core-valence double-ζ contraction level. All QM calculations were performed for all plausible spin states. For open-shell systems, QM calculations were performed using the spin-unrestricted DFT (UDFT). ReaxFF does not employ the concept of multiple spin states and is parameterized to reproduce the energy corresponding to the lowest energy spin state.

2.3 Molecular Dynamics Simulations

To evaluate the oxidation states of the metals in the M1 phase, the 4-layer periodic model was energy minimized and an NVT-MD simulation was performed. The temperature was increased from 0 K to 300 K at 4 K/ps and then the temperature was maintained at 300 K for an additional 12.5 ps of simulation time. The temperature was controlled using a Berendsen thermostat [26] with a temperature damping constant of 0.25 ps. A MD-timestep of 0.1 fs was used in this simulation.

2.4 Mechanism for Selective Oxidation of Propene by BiMoOx Catalysts

In addition to earlier work [7, 8], which explored the thermodynamics of prospective reaction pathways, we have now also examined the relevant kinetics for this chemistry [27]. The reaction barrier for conversion of propene into allyl on a Bi^{V} site was explored using a $Bi^{V}Bi^{III}{}_3O_4$ cluster model, and was determined to be 12.8 kcal/mol (TS1, Fig. 3). This barrier is ~6 kcal/mol lower in energy than the experimentally measured one, which could be explained by the relatively low concentration of Bi^{V} sites on the surface. Indeed, 6 kcal/mol would correspond to a relative Bi^{III}/Bi^{V} ratio of 1:200 at 573 K or 1:63,000 at 273 K, which seems reasonable for this surface. In addition, we find this process is highly endothermic on Bi^{III} and has a significantly higher barrier on a Mo^{VI}.

The subsequent steps, after transferring the allyl to a MoO_x site, employ a Mo_3O_9 model cluster, which has already been widely used to investigate propene oxidation on Mo-oxides. Adsorption of the allyl is found to be exothermic and almost barrierless, as expected. However, the activation energy for the second hydrogen abstraction (TS2, Fig. 1) is relatively large, 35.7 kcal/mol, which suggests that no further product formation should occur on a pure MoO_3 surface. This seems at a first glance to contradict the known chemistry of $BiMoO_x$ chemistry, where it is assumed that Mo converts the formed allyl radical to products.

However, these results potentially explain the observations of Martir and Lunsford [10]. In their experimental report, they observe that pure Bi_2O_3 generates allyl radical in the gas phase when propene is passed over the surface, the allyl radicals are rapidly scavenged (and converted to oxygenated products) when $BiMoO_x$ are used, but that if

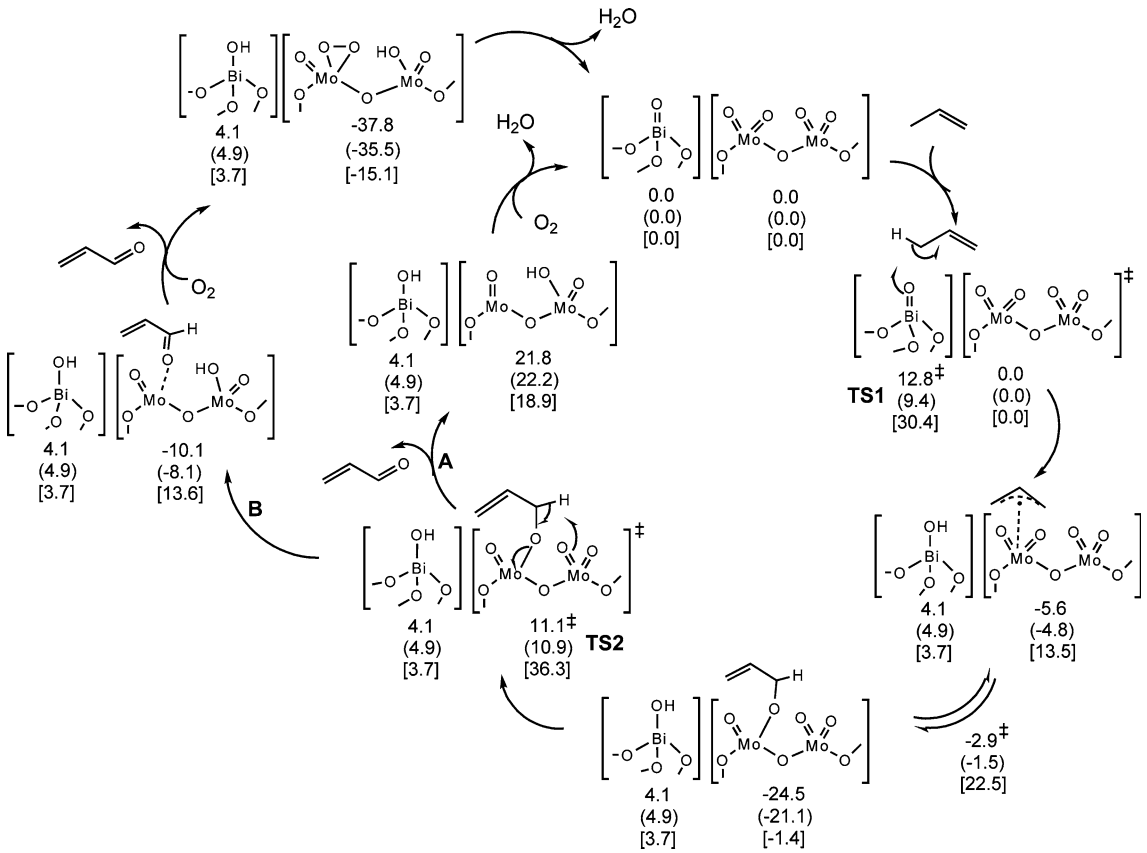

Fig. 3 Proposed mechanism and energetics for propene oxidation over bismuth molbydate catalyst. The top energy is the ΔE from the QM, the middle is $\Delta H_{0K} = \Delta E + \Delta ZPE$, and the bottom is ΔG_{593K}. All reported values are in kcal/mol

pre-generated allyl radicals are passed over pure MoO_3 no oxygenated products are observed. Martir and Lunsford [28] suggested that a synergetic effect between Mo and Bi must be responsible for the product formation, but no further information on the nature of this effect is known.

We Þnd that the direct desorption of acrolein from the cluster (Path A in Fig. 3) is energetically less favorable than the O_2-assisted acrolein desorption (Path B in Fig. 3). The kinetics for acrolein desorption suggest that re-oxidation of the reduced site signiÞcantly improves the desorption process.

2.5 Mechanism for Selective Ammoxidation of Propene by BiMoOx Catalysts

In addition to the general oxidation scheme studied above, we have investigated the mechanism of ammoxidation of propene [28]. This process involves activation of ammonia by terminal Mo=O groups to form imido species (Mo=NH), followed by propene activation, N insertion, and three subsequent hydrogen abstractions to form acrylonitrile as a Þnal product. Oxidation of propene occurs at 320 °C, but upon the addition of ammonia to the feed, ammoxidation does not start until the temperature reaches at least 400 °C [29]. Furthermore, the presence of ammonia in the feed considerably decreases oxidation rates at 320 °C as well, while both ammoxidation and oxidation occurs at 400 °C. This indicates that ammonia blocks the active site(s) required for both oxidation and ammoxidation, but can be activated or desorbed at 400 and higher.

The rate-determining step in formation of acrylonitrile is activation of propene to form a π-allylic species, which is in a rapid equilibrium with a σ-N allyl species [29, 30]. The rate determining step for conversion of N-allyl to acrylonitrile is the 2nd H (allylic) abstraction [31]. Kinetic studies show that the propene conversion rates depend on the partial pressure of NH_3/C_3H_6 [29]. At low partial pressures of feed ($pC_3H_6 = 0.041$ atm), corresponding to low conversion rates, the acrylonitrile/acrolein ratio is found to be linear function of NH_3/C_3H_6, indicating that only one ammonia molecule is involved at the N-insertion site per catalytic cycle. The major N-inserting species is a low concentration of ÔÔimido-oxoÕÕ surrounded by ÔÔdi-oxoÕÕ species 1 and 2 respectively, Fig. 4). At medium partial pressures of feed ($pC_3H_6 = 0.082$ atm; intermediate conversion conditions), the product ratio is a linear function of

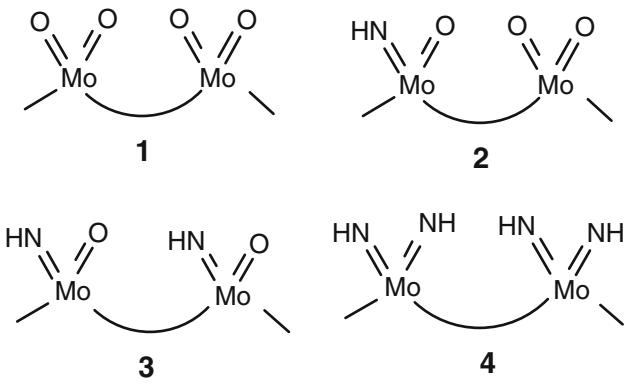

Fig. 4 Major species at different partial pressures of feed, proposed by Grasselli et al. [10]

$(NH_3)^2/C_3H_6$, corresponding to two NH_3 molecules condensed per acrylonitrile formed. In addition, there is a break in the line where the slope at lower NH_3/C_3H_6 ratios (<0.24) is 2.5 times larger than at the higher ratios. At $NH_3/C_3H_6 = 0.24$, the major surface species is ÔÔimido-oxoÕÕ (3). At high feed concentration ($pC_3H_6 = 0.14$ atm; high conversion rates), the product ratio is also a linear function of $(NH_3)^2/C_3H_6$, corresponding to activation of two ammonia at the N-insertion site per acrylonitrile formed. The major surface species present are ÔÔdi-imidoÕÕ (4).

In order to understand the details of this process, we investigated the activation of ammonia on Mo^{VI} and Mo^{V} sites to understand how it relates to reaction temperature and decrease in conversion of propene to acrolein. We also explored allyl adsorption and conversion to acrylonitrile under different pressures of ammonia to explain how different N-insertion sites affect conversion rates. As the activation of propene is believed to occur on bismuth site, we consider only the steps after the allyl generation, and assume that all later steps occur on molybdenum using the cluster model $Mo_3O_x(NH)_y$. This model has a very similar stoichiometry and connectivity of metal-oxygen bonds as those found in the crystal structure of molybdenum oxide and bismuth-molybdates.

In the oxidized form of the catalyst, molybdenum is mostly in the 6+ oxidation state, although there might also be Mo^{4+} sites resulting from reductive ammonia activation, propene oxidation to acrolein, and ammoxidation to acrylonitrile. As shown below, the net energy cost for NH_3 activation on Mo^{VI} and Mo^{V} is the same, but the energy cost for each step on Mo^{V} is greatly reduced.

2.5.1 Ammonia Activation at Mo^{VI}

A QM potential energy surface for NH_3 activation is shown in Fig. 5. Coordination of ammonia to Mo is quite exothermic ($\Delta H = -24.5$ kcal/mol), which explains the rapid decrease of propene conversion upon addition of ammonia. No oxidation can occur until NH_3 is either activated (to form a Mo=NH species) or desorbs from the surface. The barrier for the Þrst step in the activation of ammonia is 41 kcal/mol (TS1, Fig. 5), which further explains the need for higher reaction temperature. The second barrier (TS2)

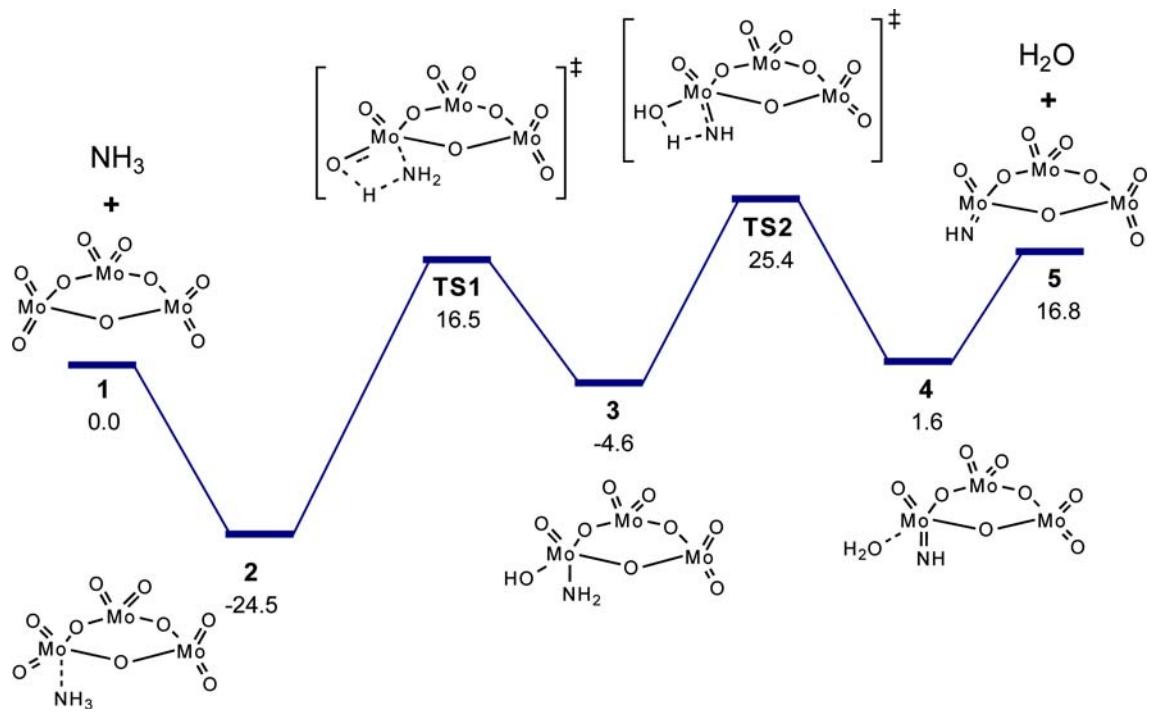

Fig. 5 Closed shell energy proÞle for activation of NH_3 on Mo(VI), ΔH_{0K} (kcal/mol)

Fig. 5), for generating H_2O, is 30 kcal/mol, and the cost of desorption of water to form ÔÔimido-oxoÕÕ species (5, Fig. 5) is 15.2 kcal/mol.

2.5.2 Ammonia Activation on Mo^{IV}

The ground state of Mo^{IV} is a triplet, and the triplet potential energy surface for NH_3 activation on Mo^{IV} is shown in Fig. 6. Ammonia adsorption on Mo(IV) is again very exothermic ($\Delta H = -35.9$ kcal/mol), which is expected considering the electronically and coordinately unsaturated Mo site. There are several possible pathways for NH_3 activation, and the most favorable pathway is one where both hydrogen atoms are transferred to the same oxo group. The highest barrier (TS6, Fig. 6) for that process is 21.8 kcal/mol, which is signiÞcantly lower than the one found for Mo^{VI}. Dissociation of H_2O from a product species (12, Fig. 6) costs 29.0 kcal/mol, and is 7.1 kcal/mol more favorable if reoxidation of catalyst occurs simultaneously with H_2O desorption (15, Fig. 6). These results suggest that once the reaction is initiated and Mo^{IV} sites start appearing in higher ratios ammonia will be activated more rapidly.

2.5.3 Ammoxidation of Allyl Radical

Since it is believed that propene activation occurs on a bismuth site, we assume that the allyl radical is the common intermediate for ammoxidation. Next, we consider the ammoxidation process under different pressures of ammonia: (1) low feed pressure corresponding to presence of ÔÔoxo-imidoÕÕ surrounded by ÔÔoxo-oxoÕÕ species (2) intermediate feed pressure corresponding to ÔÔoxo-imidoÕÕ species and ÔÔimido-imidoÕÕ species; and (3) high feed pressure corresponding solely to ÔÔimido-imidoÕÕ species.

2.5.3.1 Low Feed Pressures The doublet potential energy surface for ammoxidation of allyl radical under low ammonia pressure is shown in Fig. 7. In order to describe active sites associated with low conversion rates, we chose a Mo_3O_8NH cluster model which contains one ÔÔoxo-imidoÕÕ group surrounded by two ÔÔoxo-oxoÕÕ groups. Allyl adsorption onto the NH group is exothermic and more favorable than adsorption onto an oxo group, as was shown by Jang and Goddard,[7,8] as well as assumed by Grasselli and co-workers when deriving kinetic equations for ammoxidation [29]. The second step, corresponding to allylic hydrogen abstraction by neighboring Mo=O group, has a barrier of 29.6 kcal/mol. The last step, where H_2O is formed as a result of abstraction of the 3rd hydrogen, has a high barrier which most likely is due to reduction of Mo from 6+ to 4+ at sites where acrylonitrile and water are formed. The barrier would likely be smaller if molecular O_2 is used to re-oxidize catalyst simultaneously with the

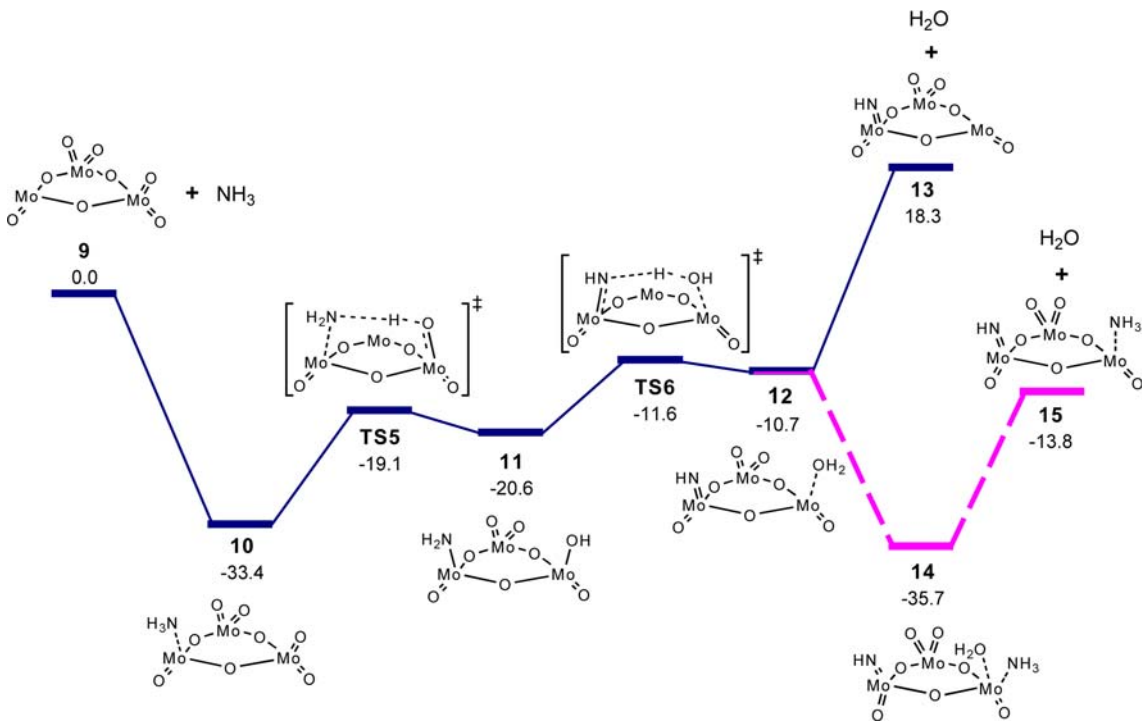

Fig. 6 Potential energy surface for activation of NH_3 on Mo(IV), ΔH_{0k} (kcal/mol). Solid blue line represents activation of ammonia using one oxo group while the broken pink line represents ammonia-assisted water desorption

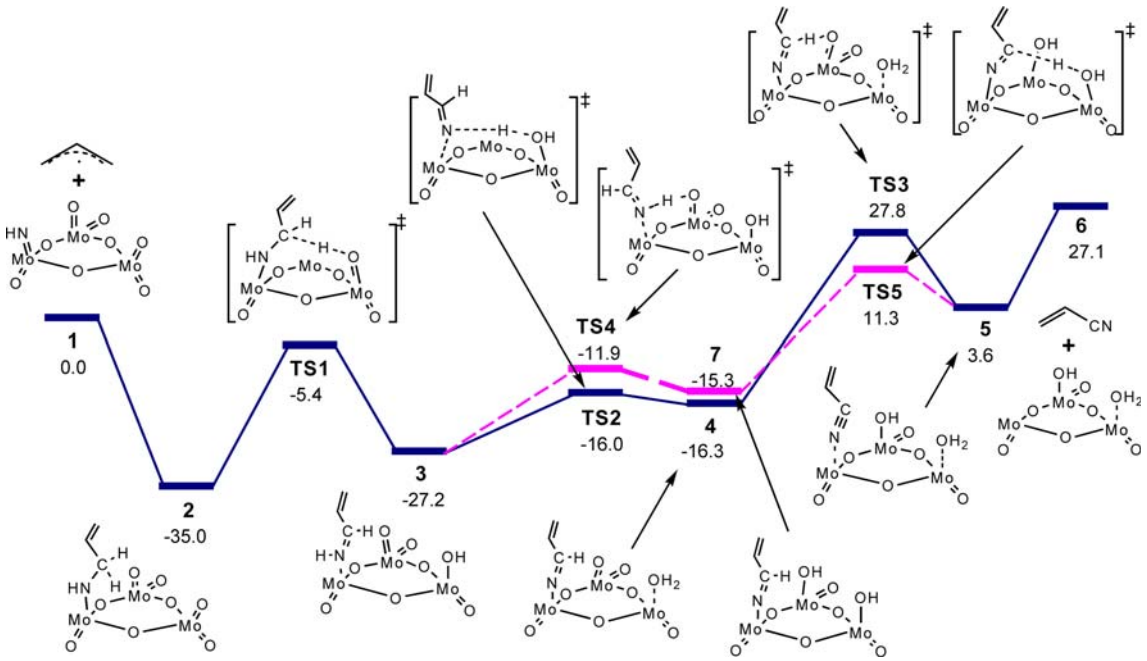

Fig. 7 Energy proÞle for allyl radical ammoxidation over Mo_3O_8NH (low partial pressure of feed). ΔH_{0K} (kcal/mol). Blue solid line represents H_2O-pathway, and pink dashed line represents 2OH-pathway

formation of acrylonitrile and water. As shown in Fig. 7, there are two possible pathways leading to the same product. The Þrst pathway involves formation of 2OH (by transferring two hydrogens to the same oxo group) while the other pathway involves formation of two OH groups (by transferring two hydrogens to two different oxo groups). Both pathways are energetically similar.

2.5.3.2 Intermediate Feed Pressures At lower NH_3/C_3H_6 ratios (<0.24), the major surface species is ÔÔoxo-imidoÕÕ (3), while at higher NH_3/C_3H_6 ratios, the major species is ÔÔimido-imidoÕÕ (4). (This is merely a reßection of the equilibrium $Mo{=}O + NH_3 \rightarrow Mo{=}NH + H_2O$ being driven to the right when a large number of ammonia is present. We studied the mechanism under lower ratios by using a $Mo_3O_7(NH)_2$ cluster model, which has two ÔÔoxo-imidoÕÕ and one ÔÔdi-oxoÕÕ species, allowing us to compare hydrogen abstractions by different groups (oxo or imido) in the same model. In addition, we have used $Mo_3O_6(NH)_3$ with three ÔÔoxo-imidoÕÕ species, which is representative of major surface species at low ratios of NH_3/C_3H_6 and intermediate feed pressures. The doublet potential energy surface for allyl ammoxidation on di-ÕÕoxo-imidoÕÕ with ÔÔdi-oxoÕÕ cluster is shown in Fig. 8. The barrier for allylic H abstraction by a neighboring imido group is 22.8 kcal/mol (TS7, Fig. 8), while the same abstraction by an oxo group is 25.7 kcal/mol. The decrease in the allylic H abstraction barrier when two ammonia molecules are activated is in agreement with experimental observations of higher propene conversion under higher pressure of ammonia, in this case an intermediate pressure of feed. If we use $Mo_3O_6(NH)_3$, the allylic H abstraction barrier is 22.7 kcal/mol.

2.5.3.3 High Feed Pressures At higher feed pressures and high NH_3/C_3H_6 ratios, the major surface species is probably a ÔÔdi-imidoÕÕ, i.e. a surface more or less saturated with imido groups. We explored ammoxidation over this species using a $Mo_3(NH)_9$ cluster model, where there are three ÔÔdi-imidoÕÕ sites. While this might be somewhat unrealistic (complete substitution of all oxygens with imidos is not expected to occur), we believe it establishes an extreme on the range of imido substituted Mo_3O_9 clusters. The barrier for allylic H abstraction on this cluster is 16.4 kcal/mol, which is lower than for the ÔÔoxo-imidoÕÕ (low NH_3/C_3H_6 ratios) case. We can thus conclude that increased imido substitution is beneÞcial to the ammoxidation rates, in accordance with experimental observation. Propene conversion is higher at higher feed pressures because the majority of surface species is ÔÔdi-imidoÕÕ and few allylic or other hydrogen abstractions occur on oxo groups for which barriers are higher (25.7 kcal/mol).

2.5.3.4 Summary of Ammoxidation We Þnd that NH_3 favorably binds to active Mo sites but the activation energy of ammonia is higher than that of propene. This is consistent with ammoxidation experiments which are carried out at higher temperatures (400–460 °C) than oxidation

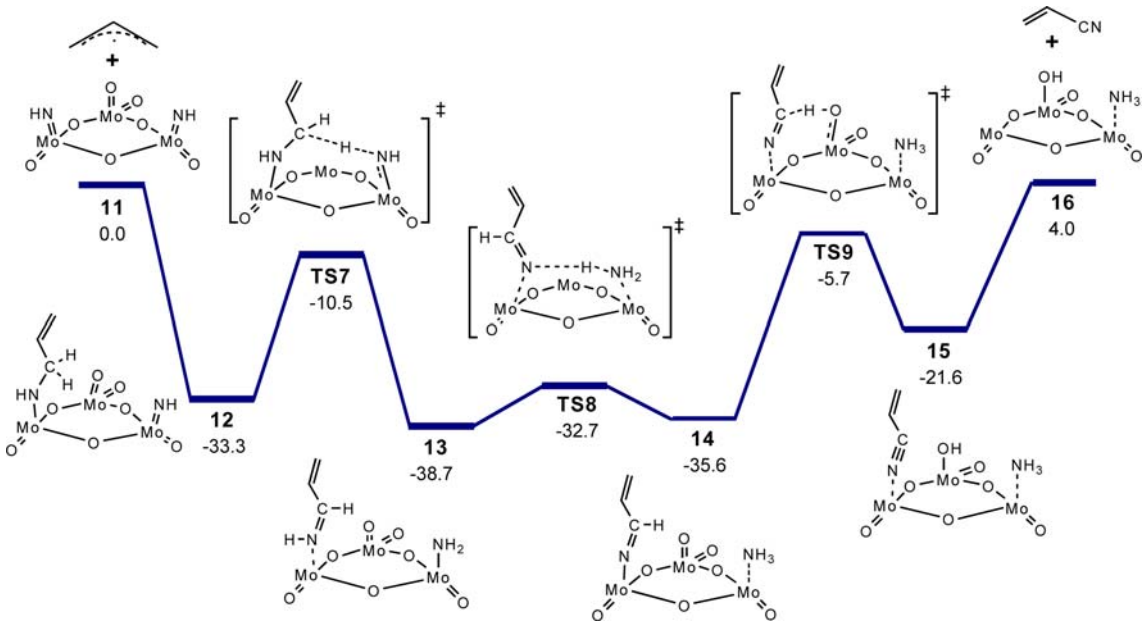

Fig. 8 Doublet potential energy surface for allyl radical conversion to acrylonitrile over $Mo_3O_7(NH)_2$ (intermediate partial pressure of feed), ΔH_{0K} (kcal/mol). The barrier for the allylic hydrogen abstraction (TS7) is 6.8 kcal/mol lower than the corresponding barrier (TS1) at low partial pressures of feed, in agreement with experiment

experiments (300Ð450°C). In addition, the conversion of propene depends on the partial pressure of feed. As the pressure increases, the turnover rate increases because the barrier for the 2nd hydrogen abstraction decreases (Table 1), in accordance with experimental observations [29].

Table 1 Barrier (ΔE) for 2nd H abstraction (rate-determining step for allyl conversion)

Number of NH groups	Barrier for 2nd H abstraction (kcal/mol)	Conversion of C_3
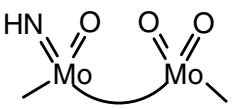 **2**	33.0	Low
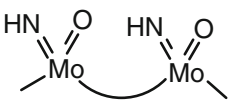 **3**	25.6	Medium
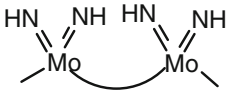 **4**	18.6	High

2.6 Mechanisms for Oxidative Dehydrogenation of Propane by V_2O_5 Catalysts

The proposed mechanism for propane activation on MMO involves the *oxydehydrogenation of the propane* to form propyl radical. In the propylene mechanism, a hydrogen migrates onto an oxygen attached to bismuth, but the chemistry with propane is complicated by the fact that an additional two hydrogens must Þrst be removed to give a propene intermediate. These Þrst two hydrogens are most likely removed through similar processes, although most likely by metals other than Mo. Currently the best oxydehydrogenation (ODH) catalysts are vanadia (V_2O_5) based, which might explain the presence of V in existing propane MMO catalysts.

To this effect, we have studied the vanadium oxide catalyzed ODH conversion of propane to propene through DFT calculations on a Þnite V_4O_{10} cluster (Fig. 9) [32]. We found that the key step is the initial hydrogen abstraction by the vanadyl (V=O) group to form a V^{IV}ÐOH radical site and an *iso*-propyl radical, which binds to an adjacent VÐOÐV site (B in Fig. 9). This step occurs through a linear OÐHÐC transition state with a calculated energy of 23.9 kcal/mol, which is very close to the experimental ΔG value of 27.0 kcal/mol [37, 38].

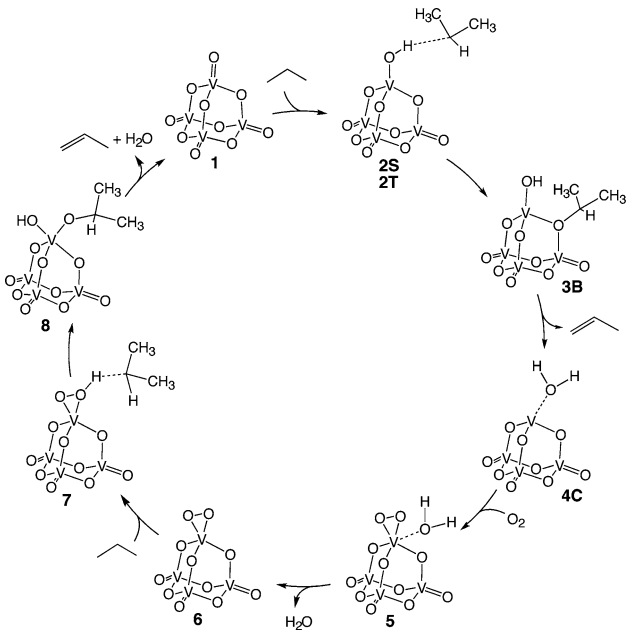

Fig. 9 The catalytic cycle for propane ODH on V_4O_{10} derived from QM calculations. We refer to this as the single site vanadyl activation, functionalization, and reoxidation mechanism (SS-VAFR)

Subsequently, this *iso*-propyl is converted to the propene product by beta-hydride elimination to form either a second V^{IV}ÐOH group or the direct formation of V^{III}ÐH_2O. No facile reoxidation pathway could be found from the V^{IV}Ð OH groups. However, we assume that hydrogen transfers should be facile on the oxide, and thus the V^{IV}ÐOH/V^{V}Ð OH sites are in equilibrium with V^{III}-OH_2/V^{V}=O. Furthermore, while we Þnd that the H_2O bound to a V^{III} site is too stable to desorb by itself, binding of gaseous O_2 to this site dramatically decreases the energy for H_2O desorption from 37.8 to 12.9 kcal/mol, while forming a cyclic V_2O_2 peroxide (4C to 6 in Fig. 9). This peroxide activates the CÐH bond of a second propane to form a second propene (with a lower reaction barrier), which eventually regenerates the original V_4O_{10} cluster. These results are in agreement with experimental barriers and mechanistic studies [33, 37, 38].

In our cluster model, we Þnd that only vanadyl oxygens (V=O) are used as the reactive site for CÐH activation, while the bridging oxygens (VÐOÐV) serve to stabilize the *iso*-propyl radical. We refer to this mechanism as the Single-Site Vanadyl Activation, Functionalization, and Reoxidation mechanism (SS-VAFR). This SS-VAFR mechanism should be directly applicable to propane ODH on the supported vanadium oxide catalysts where only monovanadate (VO_4) species are present. For pure surfaces, we expect that V=O is also used to stabilize the iso-propyl radicals, as shown by Fu et al. in a recent study of this mechanism on the pure surface using periodic DFT [33].

Apart from the participation of a neighboring V=O oxygen, ours and FuÕs mechanisms are very similar in terms of barriers both for the overall process and for the individual steps.

3 Application of ReaxFF Reactive Force Field to MMO Catalyst

3.1 Development of a ReaxFF Potential for Metal Oxides and their Catalytic Interactions with Hydrocarbons

To develop ReaxFF parameters for metal oxides and their catalytic interactions with hydrocarbons we performed QM-simulations on a wide range of systems covering the physical and chemical properties of the metal oxide/hydrocarbon system. This training set covers stable and unstable metal oxidation states, low and high energy metal and metal oxide coordinations, equations of state for relevant metal and metal oxide phases, charge distributions and reactant/product/intermediate/transition state energies for dehydrogenation, hydrocarbon oxidation/ammoxidation and metal re-oxidation reactions. After completing this QM-based training set, we parameterize the ReaxFF description for the metal oxide materials, ensuring that the Þnal parameters retain their quality with regards to the hydrocarbon training set [14].

Figures 10Ð12 provides examples of the QM-data used to parameterize ReaxFF. Figure 10 shows the QM and ReaxFF results for various metal oxide condensed phases, covering all the oxidation states relevant to hydrocarbon oxidation catalysis. ReaxFF successfully reproduces the energy differences between these oxidation states and also matches the QM energy/volume relationship, indicating that it can describe both the physical behavior and the redox chemistry related to these metal oxides. Figure 11 compares the QM and ReaxFF results for a full catalytic cycle, including dehydrogenation, hydrocarbon oxidation and catalyst regeneration, for propane conversion on a V_4O_{10}-cluster. ReaxFF provides a good reproduction of the QM-stabilities of all the stable and transition state conÞgurations encountered during this catalytic cycle, indicating that the method is suitable for describing the kinetics of metal-oxide catalyzed hydrocarbon oxidation. Figure 12 shows the QM and ReaxFF comparison for distortion of the MÐOÐN angle in various MMO clusters. The angle distortion was performed by simultaneously Þxing both MÐOÐN angles in the clusters while optimizing the remaining coordinates. The resulting energy proÞle was used to optimize the valence angle parameters for MMO systems. ReaxFF provides a good description of the strain involved in distorting the various MÐOÐN angles.

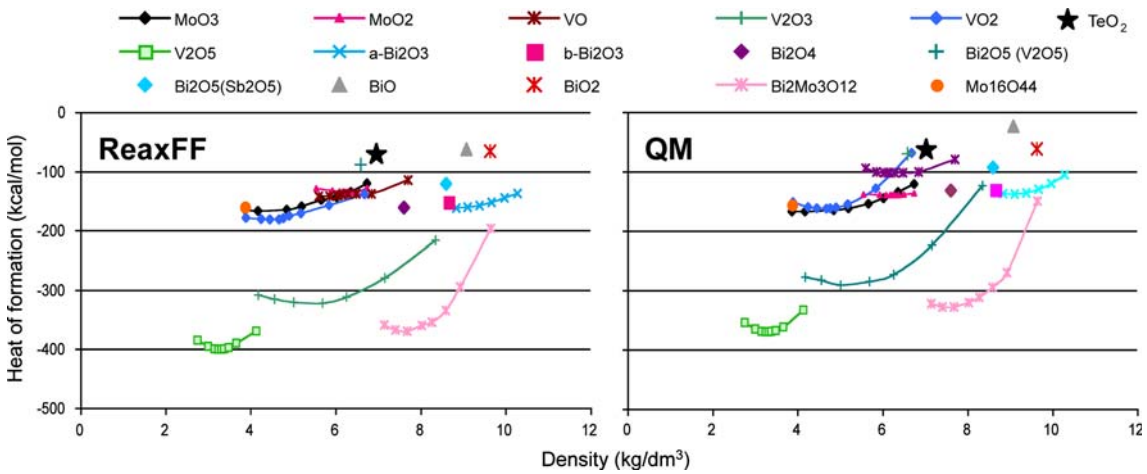

Fig. 10 ReaxFF and QM equations of state for metal oxides including W^{VI}, V^{IV}, V^{V}, Bi^{III}, Bi^{V}, $Bi^{III}Bi^{V}$, Te^{IV}, Mo^{VI}, Mo^{IV} oxidation states

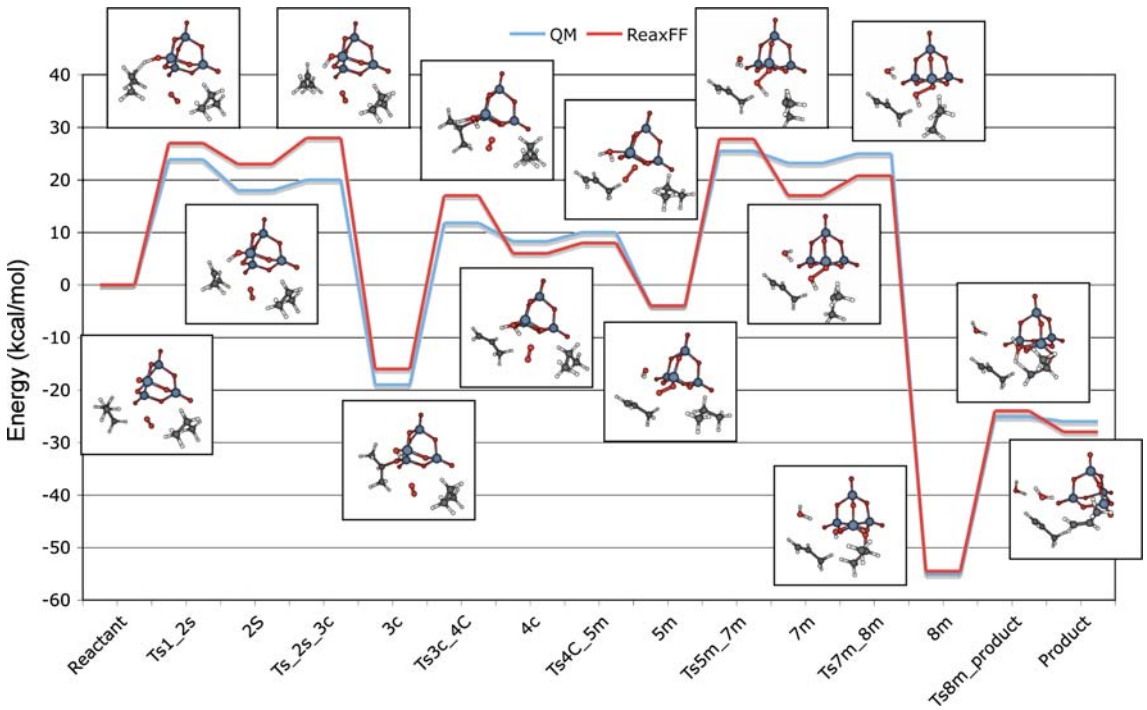

Fig. 11 QM- and ReaxFF reaction pathways for the selective oxidation of propane on a V_4O_{10} particle

3.2 Application of ReaxFF to the Study of the Reaction Dynamics of Metal Oxide-Catalyzed Hydrocarbon Oxidation

Using the ReaxFF force Þeld for MMO, we have simulated the high-temperature dynamics of hydrocarbon oxidation on single metal oxide surfaces. Vanadium oxide is known to be a highly active, but rather non-selective, hydrocarbon oxidation catalyst [16]. In our previous work [34], we exposed a V_2O_5 (001) surface to propene. This system was equilibrated at 500 K, after which the hydrocarbon phase was heated up linearly to 2,000 K. Initial reactivity (oxidative dehydrogenation) was observed at a hydrocarbon temperature of around 1,000 K; continuous heating eventually resulted in desorption of allyl radicals and eventual oxidation to acrolein and a range of other oxidized hydrocarbons. These observations are in good agreement with both the high activity and the low selectivity of the V_2O_5 catalyst. Similar simulations on a MoO_3 catalyst show this metal oxide phase to be considerably less active than V_2O_5 [5, 34] which is in good agreement with experiment [35]. Further simulations demonstrated that

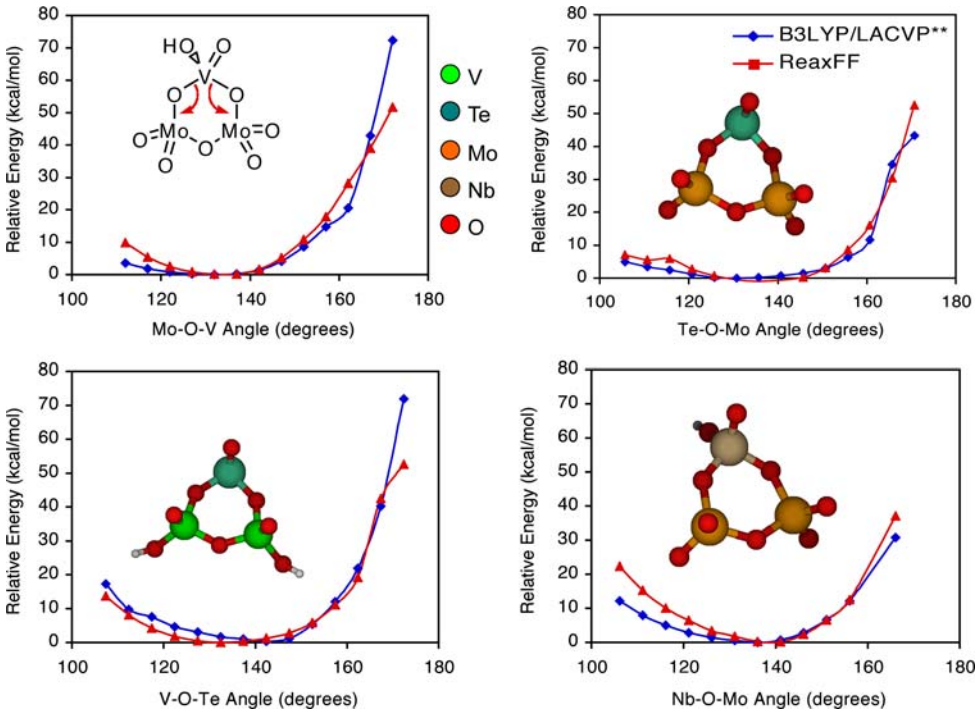

Fig. 12 QM (blue line) and ReaxFF (red line) energies for distortion of MÐOÐN angle in MMO clusters. At each point, both MÐOÐN angle in the cluster are distorted while relaxing the remaining degrees of freedom

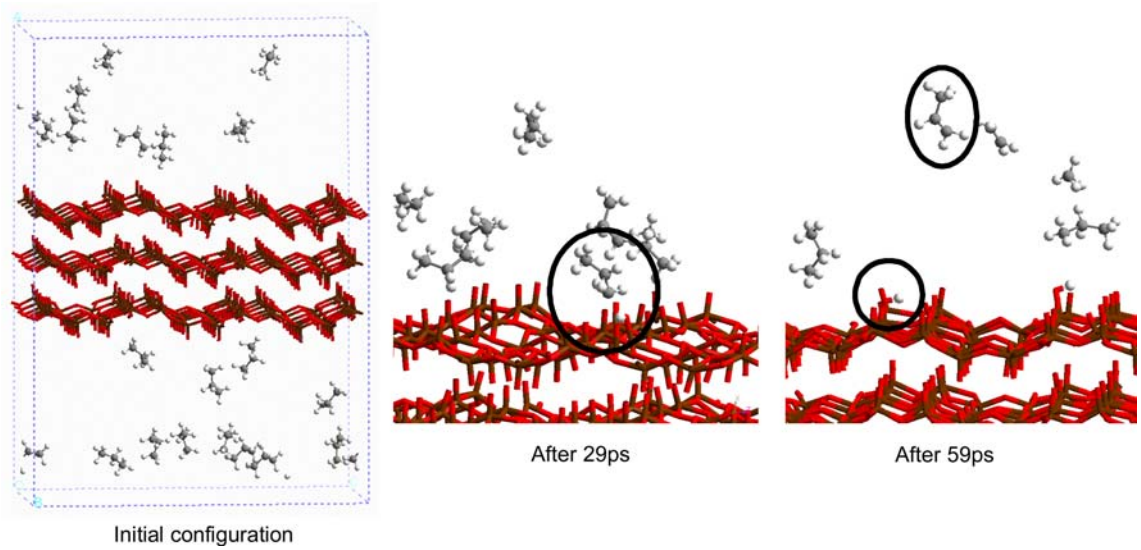

Fig. 13 System conÞgurations observed during high-temperature ReaxFF dynamics simulations of the propane/V_2O_5 interface

V_2O_5 is also capable of oxidative dehydrogenation of propane to form propene (Fig. 13), and that the MoO_3 surface is virtually non-reactive towards propane. Both of these results are supported by experiment [36Ð38]. We observed that the activation of the propyl bond occurs through a V=O group on the V_2O_5 (001) surface. This is followed by a second hydrogen abstraction by a different surface V=O group to form the propene product. This simulation illustrates the capability of ReaxFF to simulate the ODH of alkanes.

3.3 Composition and Structure of MMO from ReaxFF

Understanding the intimate interplay between the various oxidation states of the multiple metals comprising the MMO catalyst as well as the synergistic effect of the catalyst phases is critical to improving properties such as activity and selectivity. The structures of the three crystalline phases comprising the MoÐVÐNbÐTeÐO catalyst were recently reported and include the orthorhombic M1 phase ($Mo_{7.8}V_{1.2}NbTe_{0.94}O_{28.9}$), the pseudo-hexagonal M2

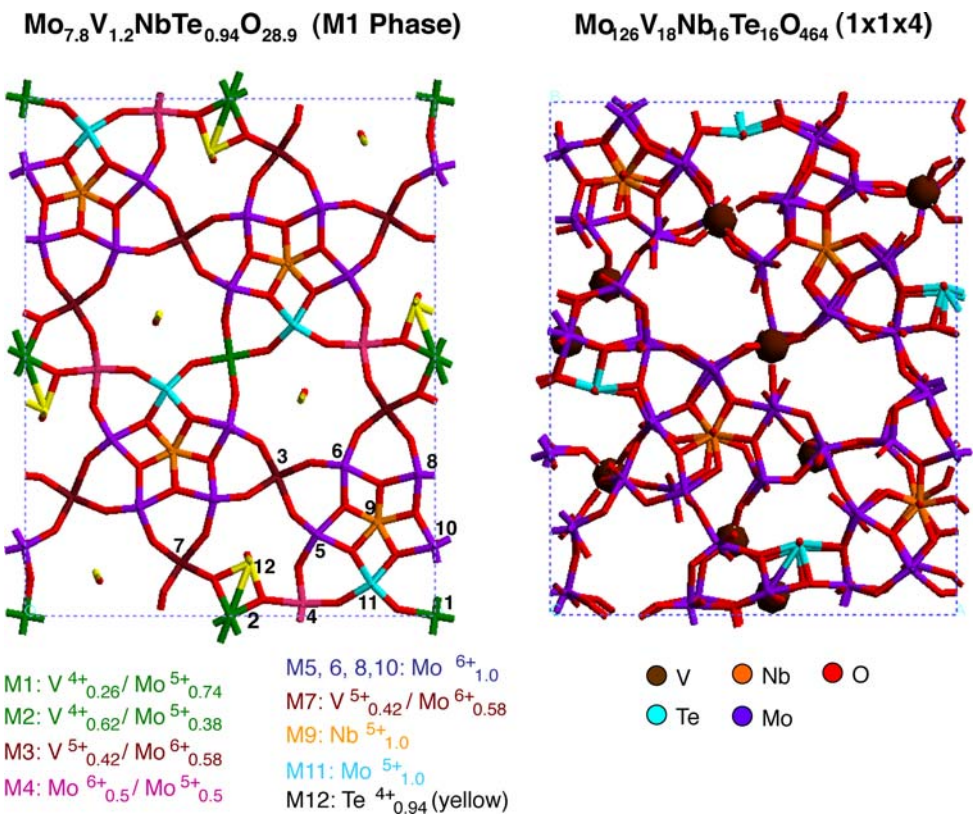

Fig. 14 Experimental disordered structure (left) and ReaxFF minimized structure (right) of one possible distribution of atoms in a 4-layer periodic model that exhibits a well-ordered unique structure with diffraction intensities consistent with experiment

phase ($Mo_{4.67}V_{1.33}Te_{1.82}O_{19.82}$), with a trace amount of the monoclinic $TeMo_5O_{16}$ phase [11]. It is generally accepted that the M1 phase is responsible for activating propane, most likely converting it to propene, and that the M2 phase does not activate propane but can selectively convert propene to acrylonitrile.

Experimental work by DeSanto et al. [39] has shown that grinding of the layered M1 phase results in higher conversion rates indicating that the [001] surface contains the active site. Compared with the bulk crystal, the surface contains a slightly lower concentration of V and a slightly higher concentration of both Nb and Te [40]. It has been proposed that Nb occupies the same crystallographic sites as V and that it may also stabilize Te at the surface. Unfortunately, MMO catalyst preparation is difficult and can be affected by many factors including the method of preparation and the calcination conditions resulting in poor reproducibility. Slight variations in the fractional occupancies of the metals does not alter the structure of the catalyst but can have an important impact on the activity/selectivity of the catalyst [41].

The reported crystal structures involve several positions with fractional occupation but our calculations require whole atoms. Hence, starting with the crystal structure, we have prepared supercells that are structured to be compatible with the observed diffraction intensities, but featuring full occupation. Starting with a $1 \times 1 \times 2$ unit cell containing Mo, Nb, and Te, we start by exchanging each Mo at the M2 position (Fig. 14) with V and minimizing the structure using the ReaxFF force field to find the energetically most stable positions for V occupancy. The most stable structure consists of a V in the first layer bridged through an oxygen to a Mo in the second layer of the unit cell. Due to the size of the unit cell, the resulting occupancy at the M2 position is 0.5 compared to the experimentally determined value of 0.62. In the future, we could obtain exact experimental occupancy by using a larger unit cell. This process is repeated for the remaining positions with Mo/V partial occupancy. The final occupancy with respect to V at positions M1, M3, and M7 are 0.5, 0.25, and 0.25, respectively. Recent structural characterization by Murayama et al. [42] of a pure M1 phase found that the Te is localized in the hexagonal channels. Thus, we have employed 100% Te occupancy at position M12 in the hexagonal channels leaving the heptagonal channels devoid of tellurium in our model of the M1 phase. Figure 14 shows a representation of our model of the M1 phase. This structure has been minimized using ReaxFF and does exhibits a well-ordered unique structure with diffraction intensities consistent with experiment. This method for removing the fractional occupancies in the MMO phases produces a model that can be used to perform MD studies to study local structures and reaction dynamics. We will do this for a number of choices of the distribution

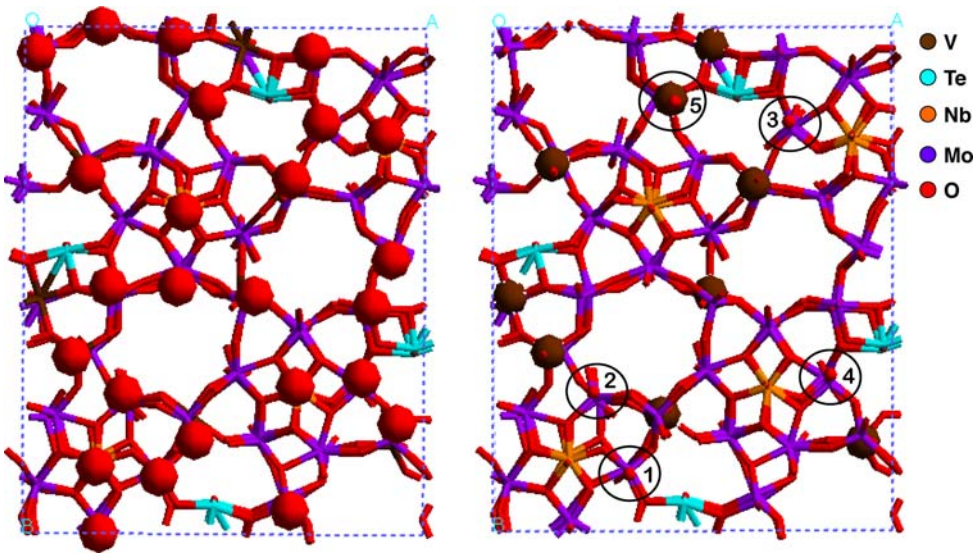

Fig. 15 ReaxFF minimized structure of 4-layer periodic slab (001) of the M1 phase where the red balls in the image on the left indicate positions of surface oxo groups and the image on the right indicates the five most reactive oxo groups

of atoms over the supercells to determine an ensemble of 3D structures where each exhibits diffraction intensities consistent with experiment.

In order to study the reactivity of the surface of the M1 phase, we created an initial periodic slab (001) that retained the maximum number of oxygens at both surfaces. Each oxygen is removed successively and the surface minimized to determine the energy for the reaction: Slab → Slab (without O) + ½ O_2. If the products are more stable than the reactant in this equation, the oxygen is permanently removed. The molecular formula for the resulting 4-layer periodic (001) slab is $Mo_{126}V_{18}Nb_{16}Te_{16}O_{478}$ and the structure is shown in Fig. 15. In order to study the reactivity of the surface oxo-groups, a hydrogen was bound to one oxo-group and the structure was minimized to calculate the energy for the reaction: Propane + Slab → Slab-H + Propyl. This was repeated for each of the surface oxo-groups. The five most reactive sites are shown in Fig. 15 and involve Mo=O and V=O sites. The best site (1, Fig. 15) involves a Mo^{VI}=O bound through bridging oxygens to Nb, Te, and Mo on the surface. The difference between site 1 and 2 through 4 is a neighboring vanadium in site 2 and a neighboring Mo with a reduced oxidation state in site 3 and 4. Next, we exchanged the metals at these sites (V for Mo and Mo for V), and minimized the structures but found that the reactivity did not improve. This result suggests that the local environment around the metal site may be important in determining the reactivity of an active site. In the future, we will anneal these surfaces computationally to allow reconstruction of the surface. These results can then be compared with low energy ion scattering and X-ray photoelectron spectroscopy experiments [43–45] which have shown that the catalyst surfaces are terminated with a monolayer that possesses a different elemental composition compared to the bulk.

Next, we performed an NVT-MD simulation of the bulk model of the M1 phase (Fig. 14) at 300 K to determine the oxidation state of the metals through analysis of the bonding. The number of interlayer Te–O–Te and Nb–O–Nb bonds remained constant during the simulation suggesting that the Te and Nb may provide a stabilizing influence on the structure. The oxidation state of Te was 4+ while Nb exhibited a 5+ oxidation state. We found that 93% of Mo were in the +6 oxidation state and the rest were Mo^{+5}. No Mo^{+4} were observed. In addition, 94% of V exhibited an oxidation state of +4 with only one V^{+5} present. In the ReaxFF structure at 300 K, Mo prefers to be fully oxidized as Mo^{+6} while V prefers to be slightly reduced as V^{+4}.

4 Summary

We have used QM calculations to elucidate the details of the reaction mechanisms for selective oxidation and ammoxidation of propene on bismuth molybdate catalysts. We find that propene activation occurs on a Bi^{V} site with a barrier of $\Delta E = 12.8$ kcal/mol whereas this process requires a significantly higher barrier (32.5 kcal/mol) on molybdenum oxide and is highly endothermic (50.9 kcal/mol) on Bi^{III}. This suggests that the C–H activation occurs on a relatively rare Bi^{V} sites. The subsequent exothermic adsorption of the allyl radical on Mo site offsets the endothermicity of the allyl generation. In addition, the process of acrolein desorption is aided by the reoxidation of the reduced site prior to the desorption.

From the mechanistic studies of ammonia activation, we find that ammonia activation is much easier on a reduced Mo site where the highest barrier is $\Delta E = 26.2$ kcal/mol and that after initiating (amm)oxidation, ammonia is

activated much more rapidly. The kinetics of ammoxidation revealed that the imido groups have both a direct effect in that H-abstraction by NH is always more favorable than H-abstraction by oxo group and an indirect effect where the presence of spectator imido groups lowers the H-abstraction barrier. In addition, the activation barrier for the 2nd hydrogen abstraction is signiÞcantly reduced if it is reoxidized prior to or during the last H-abstraction event. We Þnd that these results (with the exception of the V^{V} active site) are consistent with experimental observations [29Ð31].

We have also explored the ODH of propane on vanadia (V_2O_5) catalysts due to it presence in existing propane MMO catalysts. The key step for CÐH activation is hydrogen abstraction by the vanadyl (V^{V}=O) group to form iso-propyl radical and a hydroxyl group on the cluster (V^{IV}ÐOH). The barrier for this process is 23.9 kcal/mol, which is consistent with the experimental ΔG value of 27.0 kcal/mol [37, 38]. We report the complete catalytic cycle for propane conversion to propene where gaseous [3] O_2 promotes the desorption of water while simultaneously re-oxidizing the active site. This mechanism provides valuable insights into the propane ODH mechanism that may be occurring on other MMO catalysts containing V.

We have used the recently developed ReaxFF reactive force Þeld to prepare a model of the M1 phase of the existing propane MMO catalyst that removes the fractional occupancy found in the crystal structure. By successively exchanging Mo for V and minimizing the structure using ReaxFF, we have found the energetically most stable structure with occupancies and diffraction intensities that are consistent with experiment. By calculating the reactivity of the surface oxo groups, it was found that Mo=O and V=O sites were the most reactive and that the local environment at each site inßuences the reactivity. In addition, NVT-MD simulations at 300 K of the bulk structure revealed that Te^{+4} and Nb^{+5} might play a stabilizing role and that the most common oxidation state of Mo is +6 and V is 4+.

We can vary the choices for the distribution of atoms to provide a collection of 3D structures, which are consistent with experiment and can be used to examine the possible surface conÞguration and active sites of MMO catalysts. We will further use ReaxFF to simulate reactions of gas phase molecules such as O_2, NH_3, H_2O, propane and propene with these surfaces exploring in detail the structure of the low energy surfaces and how variations in these surfaces alter the performance of the catalyst as well as the function of each metal.

Acknowledgements We thank Dr. Robert Grasselli for continued encouragement and helpful discussions. The computers used in these projects were provided by ARO-DURIP and ONR-DURIP grants. Partial support was also provided by DOE (DE-AC02-06CH11357 and DE-PS36-03GO93015)

References

1. UllmannÕs Encyclopedia of Industrial Chemistry (2007) Electronic release. Wiley-VCH, Weinheim
2. Ushikubo T, Oshima K, Kayo V, Umezawa T, Kiyono T, Sawaki I (1994) Mitsubishi Kasei Corporation. US Patent # 5,281,745
3. U.S. Patents 4,746,641 (1988), 4,788,317 (1988), 4,843,055 (1989) Assigned to the Standard Oil Company
4. Blanksby SJ, Ellison GB (2003) Acc Chem Res 36:255
5. Grasselli RK (2007) 234th ACS national meeting, Boston, MA, August 19Ð23
6. Allison JN, Goddard WA (1985) III ACS symposium series No. 279. Grasselli RK, Brazdil JF (eds) Solid state chemistry in catalysis. American Chemical Society, Washington, DC, 23
7. Jang YH, Goddard WAIII (2001) Top Catal 15:273
8. Jang YH, Goddard WAIII (2002) J Phys Chem B 106:5997
9. Grasselli RK, Burrington JD, Buttrey DJ, DeSanto P, Lugmair G, Volpe AF, Weingand T (2003) Top Catal 23:5
10. (a) Swift HE, Bozik JE, Ondrey JA (1971) J Catal 21:212; (b) Grzybowska G, Haber J, Janas J(1977) J Catal 49:150; (c) Martir W, Lunsford JH (1981) J Am Chem Soc 103:3728; (d) White MG, Hightower JW (1983) J Catal 82:185
11. Desanto P Jr, Buttrey DJ, Grasselli RK, Lugmair CG, Volpe AF Jr, Toby BH, Vogt T (2004) Z Kristallogr 219:152
12. Grasselli RK (2005) Catal Today 99:23
13. van Duin ACT, Dasgupta S, Lorant F, Goddard WAIII (2001) J Phys Chem A 105:9396
14. Chenoweth K, van Duin ACT, Goddard WAIII (2008) J Phys Chem A 112:1040
15. Strachan A, van Duin ACT, Dasgupta S, Chakraborty D, Goddard WAIII (2003) Phys Rev Lett 91:098301
16. van Duin ACT, Strachan A, Stewman S, Zhang Q, Goddard WAIII (2003) J Phys Chem A 107:3803
17. Zhang Q, Cagin T, van Duin ACT, Goddard WAIII (2004) Phys Rev B 69:045423
18. Nielson KD, van Duin ACT, Oxgaard J, Deng W, Goddard WAIII (2005) J Phys Chem A 109:493
19. Cheung S, Deng W, van Duin ACT, Goddard WAIII (2005) J Phys Chem A 109:851
20. Jaguar 6.5 (2006) Schrodinger, LLC, Portland, Oregon
21. (a) Hay PJ, Wadt WR (1985) J Chem Phys 82:299; (b) Goddard WA III (1968) Phys Rev 174:659; (c) Melius CF, Olafson BO, Goddard WA III (1974) Chem Phys Lett 28:457
22. (a) Hariharan PC, Pople JA (1972) Chem Phys Lett 16:217; (b) Francl MM, Pietro WJ, Hehre WJ, Binkley JS, Gordon MS, DeFrees DJ, Pople JA (1982) J Chem Phys 77:3654
23. (a) Becke AD (1992) J Chem Phys 96:2155; (b) Becke AD (1992) J Chem Phys 97:9173; (c) Becke AD (1993) J Chem Phys 98:1372; (d) Becke AD (1993) J Chem Phys 98:5648
24. Lee C, Yang W, Parr RG (1998) Phys Rev B 37:785
25. Keith JA, Gonzales J, Oxgaard J, Goddard WA III (Manuscript in preparation)
26. Berendsen HJC, Postma JPM, van Gunsteren WF, DiNola A, Haak JR (1984) J Chem Phys B 81:3684
27. Pudar S, Oxgaard J, Chenoweth K, van Duin ACT, Goddard WAIII (2007) J Phys Chem C 111:16405
28. Pudar S, Oxgaard J, Chenoweth K, van Duin ACT, Goddard WA III (Manuscript in preparation) J Phys Chem C
29. Burrington JD, Kartisek CT, Grasselli RK (1983) J Catal 81:489
30. Burrington JD, Kartisek CT, Grasselli RK (1984) J Catal 87:363
31. Grasselli RK, Burrington JD (1984) Ind Eng Chem Prod Res Dev 23:393
32. Cheng M-J, Chenoweth K, Oxgaard J, van Duin A, Goddard WAIII (2007) J Phys Chem C 111:5115

33. Fu H, Liu Z-P, Li Z-H, Wang W-N, Fan K-N (2006) J Am Chem Soc 128:11114
34. Goddard WAIII, van Duin A, Chenoweth K, Cheng M-J, Pudar S, Oxgaard J, Merinov B, Jang YH, Persson P (2006) Top Catal 38:93
35. Grzybowska-Swierkosz B, Haber J, Janas J (1997) J Catal 49:150
36. Grzybowska-Swierkosz B (1997) Appl Catal A 157:409
37. Argyle MD, Chen K, Bell AT, Iglesia E (2002) J Phys Chem B 106:5421
38. Argyle MD, Chen K, Bell AT, Iglesia E (2002) J Catal 208:139
39. Desanto P Jr, Buttrey DJ, Grasselli RK, Lugmair CG, Volpe AF Jr, Toby BH, Vogt T (2003) Top Catal 23:23
40. Vitry D, Morikawa Y, Dubois JL, Ueda W (2003) Appl Catal A 251:411
41. Grasselli RK, Buttrey DJ, DeSanto P Jr, Burrington JD, Lugmair CG, Volpe AF Jr, Weingand T (2004) Catal Today 91Ð92:251
42. Murayama H, Vitry D, Ueda W, Fuchs G, Anne M, Dubois JL (2007) Appl Catal A 318:137
43. Guliants VV, Bhandari R, Swaminathan B, Vasudevan VK, Brongersma HH, Knoester A, Gaffney AM, Han S (2005) J Phys Chem B 109:24046
44. Guliants VV, Bhandari R, Brongersma HH, Knoester A, Gaffney AM, Han S (2005) J Phys Chem B 109:10234
45. Guliants VV, Bhandari R, Hughett AR, Bhatt S, Schuler BD, Brongersma HH, Knoester A, Gaffney AM, Han S (2006) J Phys Chem B 110:6129